Applied Catalysis B: Environmental 117–118 (2012) 292–301

Contents lists available at SciVerse ScienceDirect

Applied Catalysis B: Environmental

journal homepage: www.elsevier.com/locate/apcatb

Tailored investigation and characterization of heterogeneous {Mn,Cu}/TiO_2 catalysts embedded within a ceria-based framework for the wet peroxide oxidation of hazardous pollutants

Rodrigo J.G. Lopes*, M.L.N. Perdigoto, Rosa M. Quinta-Ferreira

CIEPQPF – Centro de Investigação em Engenharia dos Processos Químicos e Produtos da Floresta, GERSE – Group on Environmental, Reaction and Separation Engineering, Department of Chemical Engineering, University of Coimbra, Rua Sílvio Lima, Polo II – Pinhal de Marrocos, 3030-790 Coimbra, Portugal

ARTICLE INFO

Article history:
Received 19 December 2011
Received in revised form 17 January 2012
Accepted 18 January 2012
Available online 28 January 2012

Keywords:
Catalytic wet peroxide oxidation
Hazardous pollutants
SEM
XRD
TiO_2
CeO_2

ABSTRACT

In this work, novel catalyst frameworks including Mn/TiO_2–CeO_2, Cu/TiO_2–CeO_2, Mn–Ce–O, Mn–Cu–O, and TiO_2–CeO_2 were investigated for the catalytic wet peroxide oxidation of phenol-like pollutants. Aiming to gain further insights into the heterogeneous catalysis of manganese and copper metals supported on titanium and cerium oxides, the abatement efficiency was evaluated under different operating conditions and in terms of individual phenolic compounds depletion. Here, Mn/TiO_2–CeO_2 was found as the most active promoter for the highest detoxification rate. Second, pH profiles and reaction intermediates unveiled a free-radical mechanism and underlined the synergism behavior in catalytic wet peroxide oxidation. The titanium based oxides exhibited the strongest catalytic stability by the quantification of metal leaching and carbon adsorption. Afterwards, the integrated metal framework encompassed by Mn/TiO_2–CeO_2 and Cu/TiO_2–CeO_2 catalysts was realized in X-ray diffraction analysis and the TEM pattern gave rise to superior homogenous structures for Mn/TiO_2–CeO_2, which has been ascribed to the integration of the lanthanide into the lattice framework of titanium oxide. Finally, several sequential feed-batch trials were carried out emphasizing that 67% of pollutant conversion can be retained after long term catalytic runs.

1. Introduction

Aiming to protect hydric resources, regional and planetary environmental regulations are now more stringent to comply with the safeguard and sustainable exploitation of water systems. Notwithstanding the disposal of liquid effluents is a major concern for the management of toxic and xenobiotic pollutants, chemical, petrochemical, pharmaceutical, and agro-biochemical industries do not follow hitherto the legal directives for water sustainability. In fact, agro-based industries have been encountered several issues to avoid or at least minimize their emissions of organic and inorganic wastewaters using feasible routes via the so-called atom economy framework [1]. In order to attain this concept, efficient and sustainable processes have to be engineered to detoxify hazardous compounds in highly contaminated wastewater streams.

Aqueous wastes from agro-processing industries such as olive oil extraction and wineries have an organic pollutant load in the range of few hundred to few thousand of milligrams per liter, which confer a high-diluted stream to incinerate, nonetheless too refractory to bio-oxidize. These agro-effluents are characterized by high levels of total organic carbon (TOC) concentration (20–85 g/L), chemical oxygen demand (COD) (40–200 g/L), biochemical oxygen demand (BOD) (12–60 g/L) and total solids content (40–150 g/L) with an acidic pH (<6) [2] and are rich in dissolved and suspended organic substances such as sugars, phenols, nitrogenated compounds, organic acids, polyalcohols, and residual oil emulsion [3]. Indeed, the dark color, phytotoxicity and antibacterial properties are attributed to the high concentration of organic compounds and polyphenolic composition.

Mainly due to inherent disadvantages of physicochemical technologies (flocculation, ultrafiltration and reverse osmosis), biological processes (aerobic, anaerobic and combined systems) for the abatement of organic compounds [4], sub-critical solid-catalyzed wet oxidation (CWO) has been envisaged as an efficient route toward the sustainable remediation of liquid pollutants. More recently, wet peroxide oxidation (WPO) have becoming a competitive technology involving complete oxidation of organics in the liquid phase using hydrogen peroxide and can be coupled with the development of active and stable catalysts [5]. Whereas a considerable number of literature studies have focused on the CWO of acetic acid [6–8] and phenol [9–11], using actual industrial streams such as Bayer liquor [12], distillery wastewater [13] and

* Corresponding author. Tel.: +351 239798723; fax: +351 239798703.
E-mail address: rodrigo@eq.uc.pt (R.J.G. Lopes).

0926-3373/$ – see front matter © 2012 Elsevier B.V. All rights reserved.
doi:10.1016/j.apcatb.2012.01.025

dyeing and printing wastewater [14], few experimental and novel catalytic frameworks have been embedded in WPO technology. Several experimental studies have been accomplished to improve the catalytic activity and stability of heterogeneous oxidation catalysts to enhance the overall efficiency of catalyzed WPO. The above-mentioned efforts were devoted to transition metals including Co, Cr, Fe, Mn, Ni and supported over different materials such as pillared clays [15], CeO_2 [16], activated carbon [17], zeolite [18], SiO_2 and γ-Al_2O_3 [19]. Nevertheless, Cu, Mn, and TiO_2-based catalyzed WPO systems have not been evaluated thoroughly. Copper and manganese oxides and CeO_2-containing materials have been studied as a good alternative for the WO catalysts and supports. However, in the field of WPO those active metals can be associated with transition metal oxides and noble metals, as they will serve as an alternative benchmark to cerium oxide which enhances oxygen storage and release to improve oxygen mobility.

In the realm of environmental reaction engineering, this work is devoted for the evaluation of laboratorial and commercial catalysts based on less expensive manganese, copper and titanium oxides for the wet peroxide oxidation of liquid pollutants. The main objective of this work addresses the catalytic activity and stability for the abatement of phenol-like pollutants after the optimization of the reaction system. Major pollutants in agro-industrial wastewaters and refractory to conventional decontamination technologies [20]: syringic (4-hydroxy-3,5-dimethoxybenzoic), vanillic (4-hydroxy-3-methoxybenzoic), 3,4,5-trimethoxybenzoic, veratric (3,4-dimethoxybenzoic), protocatechuic (3,4-dihydroxybenzoic) and *trans*-cinnamic are applied to mimic the phenolic content of biochemical and agro-industrial wastewaters.

2. Experimental

2.1. Materials and catalysts

Six phenolic compounds were obtained for Sigma–Aldrich to mimic the bactericide behavior of olive oil processing wastewaters, namely: syringic, vanillic, 3,4,5-trimethoxybenzoic, veratric, protocatechuic and *trans*-cinnamic acid. TiO_2–CeO_2, Mn–Ce–O, Mn–Cu–O, Mn/TiO_2–CeO_2, Cu/TiO_2–CeO_2 catalysts were prepared by co-precipitation (CP), by mixing aqueous solutions of the respective metal salts using the corresponding metal nitrates as precursors (Riedel-de-Häen and Labsolve). The solution was poured into 200 mL of a 3 M NaOH solution. The precipitate was filtrated and washed five times with 500 ml of ultra-pure water and dried over night at 105 °C and finally calcinated at 300 °C. Aiming to evaluating the preparation technique, Mn–Ce–O and Mn–Cu–O was also prepared by wetness impregnation (IMP). This method consisted in putting in contact 40 g of the support with 200 mL of an aqueous solution of Mn metal precursor. The solution was mixed during 30 min and further dried at 105 °C. The precipitation method consisted in dissolving $Ce(NO_3)_3{\cdot}6H_2O$ in bidistilled water (0.4 M) and KOH 1 M was added dropwise up to a pH 9. The powder was dried at overnight, and then calcined in air atmosphere for 4 h. The supports were further impregnated using $Cu(NO_3)_2{\cdot}2.5H_2O$ as precursor. The solids were dried at room temperature for 24 h, then at 105 °C in air atmosphere and finally calcined in air for 4 h. The final CuO loadings of the catalysts can be found in Table 1. The dried catalyst was crushed in a fine powder (125–250 μm particle size) in order to provide with high specific surface area for reaction and calcination was carried out at 300 °C. Several catalyst loads were investigated in the range 1.5–6.0 g/L with the original and sieved catalyst diameter, d_p. Sieve analysis was carried out for measuring particle size distribution. The original size obtained from the preparation procedure was approximately 900 μm and after mechanical sieving, d_p was in the range of 250–350 μm.

Table 1
Molar composition and BET surface area of the catalysts.

Catalyst	Molar ratios	S_{BET} (m^2/g)
Mn/TiO_2–CeO_2	10 (Mn)/80 (Ti)–10 (Ce)	197.1
Cu/TiO_2–CeO_2	10 (Cu)/80 (Ti)–10 (Ce)	194.8
Mn–Ce–O	70 (Mn)–30 (Ce)	93.94
Mn–Cu–O	70 (Cu)–30 (Ce)	94.71
TiO_2–CeO_2	85 (Ti)–15 (Ce)	181.7

Different drying and calcinations temperatures were investigated to evaluate their effect on the BET areas of TiO_2–CeO_2, Mn–Ce–O, Mn–Cu–O, Mn/TiO_2–CeO_2, and Cu/TiO_2–CeO_2 catalysts. In the following combinations 105 °C/300 °C, 90 °C/400 °C, 105 °C/400 °C, the drying temperature increase from 90 to 105 °C had no influence on the surface area which remained fixed at 93.94 m^2/g for the manganese/cerium catalysts. However, the increase in the calcination temperature from 300 to 400 °C affected negatively the BET surface area by reducing it from 106.2 to 93.94 m^2/g. Bearing in mind that higher calcination temperatures produce catalysts with lower surface areas, the calcination stage at 300 °C was carried out to prepare all the laboratory-made catalysts. The BET surface areas for the titanium-based catalysts were 181.7, 197.1 and 194.8 m^2/g for TiO_2–CeO_2, Mn/TiO_2–CeO_2, and Cu/TiO_2–CeO_2, respectively. The molar composition and BET surface area of the catalysts are shown in Table 1.

2.2. Oxidation reactor and procedure

The oxidation experiments were performed in a 316-SS high-pressure 1 L autoclave (Parr Instrument Company, model 4531M) equipped with two six-bladed mechanically driven turbine agitator and a PID temperature controller (4842 Parr model) described elsewhere [21]. The thermocouple and liquid sample line are immersed in the solution and the system allows operating conditions up to 130 bar and 350 °C being air flow controlled by an electronic mass flow controller (Hastings). The solution of phenolic acids (1200 mg/L, 200 mg/L for each phenolic acid: syringic, vanillic, 3,4,5-trimethoxybenzoic, veratric, protocatechuic and *trans*-cinnamic) was introduced in the system with: 10 mL of hydrogen peroxide (30%, w/w), the powder catalyst (1.5–6 g/L), and preheated up to the operating temperature (110–150 °C) under different agitation velocities from 100 to 400 rpm. The solution of six phenolic acids was prepared with 200 mg/L which gives 1200 mg/L. This means that total organic carbon concentration equivalent to 200 mg/L is 109.09, 114.29, 113.20, 118.66, 109.10, 145.91 mg C/L for syringic, vanillic, 3,4,5-trimethoxybenzoic, veratric, protocatechuic, and *trans*-cinnamic acids. Therefore, the hydrogen peroxide reagent was in excess for a pollutant solution having 710.24 mg C/L. The gas-side mass-transfer resistance was estimated to be negligible because of the very high diffusivity in the gas phase. In what regards the liquid-phase mass-transfer resistance, the rate of oxidation was found to be independent of the impeller speed in a range of 400 rpm, indicating that there were no resistances associated with the oxygen transfer. The oxidation experiments were therefore carried out at 400 rpm. Identical abatement efficiencies were observed when the solid was used in the original form obtained from the preparation procedure (particle size approximately up to 900 μm) and when using particles in the range of 250–350 μm. The oxidation runs were then performed by selecting these optima values.

For the catalytic activity studies in terms of individual phenolic compounds depletion, six solutions of each phenolic acid with a concentration about 200 mg/L were prepared. Pure air (99.999%) was introduced into the system up to the operating pressure and preserving it at 5 or 20 bar total pressure during the catalytic runs.

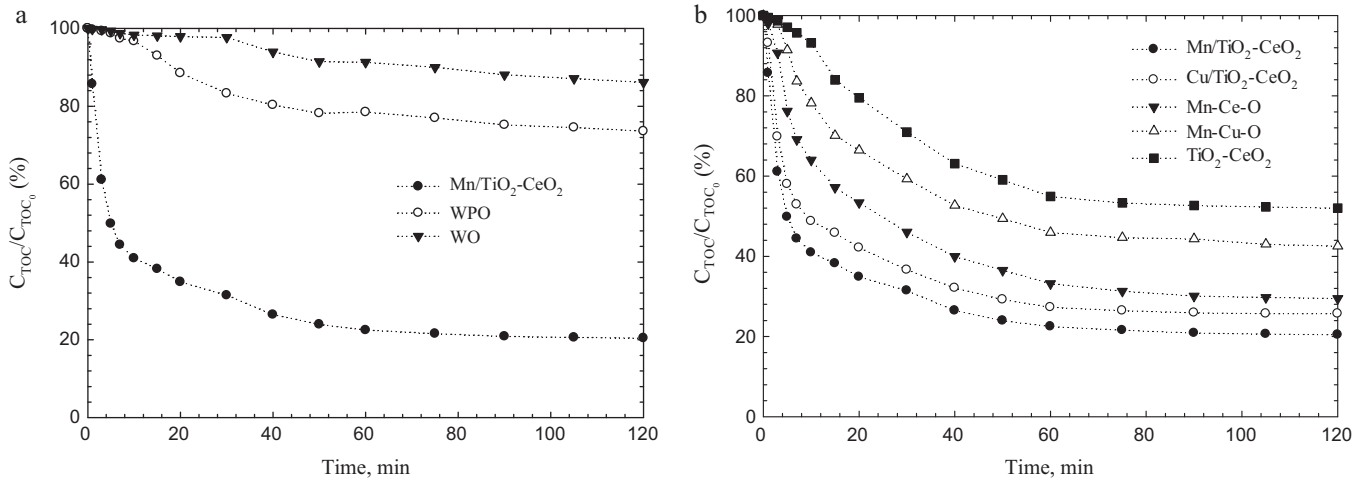

Fig. 1. Normalized total organic carbon concentration as a function of reaction time for different (a) non-catalytic (wet oxidation – WO, and wet peroxide – WP at 150 °C, 5 bar air) and (b) laboratory-made catalysts: TiO_2–CeO_2, Mn–Cu–O, Mn–Ce–O, Cu/TiO_2–CeO_2, and Mn/TiO_2–CeO_2 6 g/L, at 150 °C, 5 bar air.

The "zero" time for reaction was taken at the first injection of oxidant. Samples were withdrawn periodically from the reactor and special attention was given to the liquid sampling procedure to avoid contamination of the samples and losses of the liquid phase and/or catalyst. Liquid samples were immediately filtered with a 316-SS filter with 0.5 μm pore sizes (Swagelok) to avoid catalyst particles in the samples withdrawn from the reactor and then analyzed for total organic carbon.

2.3. Analytical techniques

Intermediate oxidation compounds were analyzed in a *Knauer HPLC system* equipped with a *WellChrom K-1001 pump*. The oven from *Jones Chromatography* (model 7971) was set at 75 °C and a SS-Column 300 mm × 8 mm inside diameter was used (10 μm particle size of a sulfonated cross-linked styrene-divinylbenzene copolymer). 100% of 0.01 N H_2SO_4 at a flow rate of 1 mL/min was used as the mobile phase. The injection volume was 20 μL while detection was typically at 280 nm. Blank samples were run between two consecutive HPLC runs to ensure that no residuals from the previous run were carried over to the next one. Both the standards and the samples were periodically run in duplicate to test the reproducibility of the measurements.

Elemental analysis was used to detect carbon adsorption in catalysts with a *Fisons Instruments EA 1108* CHNS-O equipped with a pre-packed ox/red quartz reactor, operating with a flash combustion and using a thermal conductivity detector (TCD); standard solutions of phenanthrene, sulfanilamide, and BBOT (2,5-bis(5-*tert*-butylbenzoxazol-2-yl)thiophen) were obtained from Fisons Instruments. *Atomic absorption* in a spectrometer *Perkin-Elmer 3300*, with hollow cathode lamps (Cathodeon) and standard solutions from BSB-Spectrol, was used to measure the leaching of manganese to the liquid phase.

TOC was measured with a *Shimadzu 5000 TOC Analyser*, which operates based on the combustion/nondispersive infrared gas analysis method. The parameter uncertainty in TOC measurement, quoted as the deviation of three separate measurements, was never larger than 2% for the range of the TOC concentrations. pH was monitored along the reactions with a HANNA instrument-HI8711E.

The fresh and spent catalysts were characterized at different scales/magnifications by scanning electron microscopy (SEM) with a *JEOL JSM-5310* and by X-ray powder diffraction (XRD) analysis using *Philips PW 3040/00 X-Pert* analyzer. The catalyst Brunauer–Emmet–Teller surface area (S_{BET}) was determined using nitrogen (−196 °C) with an accelerated surface area and porosimetry analyzer (*ASAP 2000*, *Micromeritics*). Porosity, pore size distribution were determined by mercury porosimetry (*Pore-sizer 9320*, *Micromeritics*). Transmission electron microscopy (TEM) measurements were performed on a *TECNAI G² 20 S-TWIN* transmission electron microscopy. It allows flexible high tension values (20, 40, 80, 120, 160, 200 kV) and use LaB_6 or W emitter as the electron source. The TEM point and line resolutions are 0.24 and 0.144 nm, respectively, whereas the minimum focus step is 1.8 nm. The TEM magnification range is 25×–1030k× while the STEM magnification range is 100×–5 M×.

3. Results

3.1. Catalytic activity and oxidation parameters

The catalytic activity of laboratory-made catalysts was evaluated in terms of abatement efficiency of the phenolic acids mixture. The normalized total organic carbon concentration is shown in Fig. 1a under different oxidation environments such as single wet oxidation (WP), single wet peroxide oxidation (WPO) and Mn/TiO_2–CeO_2-catalyzed wet peroxide oxidation. After 2 h, only 13.9% in TOC abatement was attained with wet oxidation and 26.4% for wet peroxide oxidation. Therefore, at 150 °C and 5 bar of air, the non-catalytic treatments were not able to mineralize efficiently the total organic carbon content of the phenolic solution. Nevertheless, when adding 6 g/L of Mn/TiO_2–CeO_2 to the oxidation system, 77.5% of total organic carbon conversion was obtained after 1 h reaction time being that the removal efficiency had increased up to 79.6% after 2 h. Consequently, wet air oxidation or wet peroxide oxidation are not likely feasible for the pollution abatement of phenol-like hazardous species without the application of an active catalyst.

The total organic carbon conversion of the acidic wastewater accomplished with laboratory-made catalysts: TiO_2–CeO_2, Mn–Ce–O, Mn–Cu–O, Mn/TiO_2–CeO_2, and Cu/TiO_2–CeO_2 were plotted in Fig. 1b. Having considered the above-referenced catalysts, the complete range of these oxidation experiments led to TOC reductions higher than those obtained in the experiments in the absence of a solid catalyst, see Fig. 1a. This fact pointed out that the presence of a catalyst is of paramount significance for the oxidation of phenolic wastewaters. Indeed, after 120 min of reaction time the abatement efficiencies were 47.9, 57.5, 70.5, 74.3, and 79.6% for TiO_2–CeO_2, Mn–Cu–O, Mn–Ce–O, Cu/TiO_2–CeO_2, and Mn/TiO_2–CeO_2, respectively. In

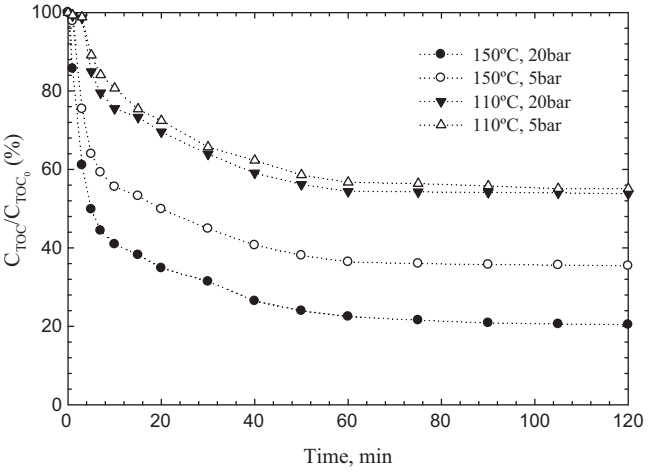

Fig. 2. Normalized total organic carbon concentration as a function of time for different temperatures (110, 150 °C) and different operating pressures (5, 20 bar) and 6 g/L of $Mn/TiO_2–CeO_2$.

fact, after 1 h of reaction, the following increasing order of detoxification efficiency was achieved with the previous catalytic treatments: $TiO_2–CeO_2$ (45.0%), Mn–Cu–O (54.1%), Mn–Ce–O (66.8%), $Cu/TiO_2–CeO_2$ (72.3%), and $Mn/TiO_2–CeO_2$ (77.5%). As long as the catalytic activity can depend upon the catalyst preparation method, the abatement of phenolic solutions was carried out over manganese/cerium oxides either prepared by wetness impregnation or co-precipitation. The higher difference in terms of TOC abatement for the two catalyst preparation methods, co-precipitation and wetness impregnation, was 1.2% in terms of normalized total organic carbon concentration. Here, the manganese and copper metals supported on titanium/cerium oxides did not confer distinct decontamination rates in terms of total organic carbon conversion, so the remainder of the discussion is centred on intrinsic operating variables inherent to wet air and wet peroxide oxidation.

As can be seen from Fig. 1b, a considerable difference between the single titanium/cerium and manganese or copper titanium/cerium based catalysts were attained at 150 °C and 5 bar air. On condition that the catalyst synthesis method was responsible to roughly lead to the same TOC conversion, the $Mn/TiO_2–CeO_2$ catalyst was very active during the first 30 min of reaction demonstrating better results with higher than 75% in TOC conversion, while the $TiO_2–CeO_2$ exhibited the lowest detoxification efficiency below 30% after the same oxidation time. In addition, the $Cu/TiO_2–CeO_2$ catalyst appeared listed after $Mn/TiO_2–CeO_2$ which have revealed that these two metals are efficient catalytic promoters when combined with the $TiO_2–CeO_2$ support. It should be stressed out that the molar composition of these laboratory-made catalyst formulations are identical and can be also intensified after enriching the metal content with manganese instead of copper. Here, more than 5% of efficiency improvement was detected from 72.3 to 77.5% for $Cu/TiO_2–CeO_2$ and $Mn/TiO_2–CeO_2$, respectively. The manganese metal revealed a prominent outcome in the carbon content depletion in comparison with the copper metal.

The influence of temperature and pressure on the catalytic wet peroxide oxidation using the $Mn/TiO_2–CeO_2$ catalyst is plotted in Fig. 2. The normalized total organic carbon concentration of the phenolic acids mixture obtained with different temperatures (110 and 150 °C) and different pressures (5 and 20 bar) highlighted that oxidation temperature has more effect than the operating pressure. Fig. 1a has depicted how the oxidant under non-catalytic conditions can mineralize the TOC concentration so even when the experimental runs was accomplished under thermolysis conditions the decontamination of phenol-like pollutants does not occur with relevant extension, which means that the oxidant has an important role in the process. Accordingly, when carrying out the experiment at 110 °C and 20 bar, the TOC conversion was 46.2% whereas at 150 °C and 20 bar it was 79.6%, after 1 h reaction time. Hence, a temperature increment of 40 °C resulted in an extensive improvement of the reaction rate during the initial reaction time. Conversely, maintaining the temperature at 150 °C and with an increase of 15 bar, the TOC removal changed from 64.6 to 88.4% showing that an increase of operating pressure affects differently the TOC depletion profiles. Nonetheless, the effect of oxidation pressure on the carbon content removal was attenuated along the last hour reaction time until the influence of both operating variables remained equivalent in terms of TOC conversion for residence times longer than 60 min, particularly at the highest oxidation temperature, 150 °C.

3.2. Catalytic activity in terms of individual phenolic compounds depletion

Bearing in mind that the transition metal may confer distinctive reaction pathways, the specific concentration of syringic, vanillic, 3,4,5-trimethoxybenzoic, veratric, protocatechuic and *trans*-cinnamic acids was monitored by HPLC analysis along the catalytic oxidation of each individual phenolic acid. In this ambit, six solutions of each phenolic acid with a concentration about 200 mg/L were prepared and for each catalytic run a single phenolic acids solution was loaded into the batch reactor. In Fig. 3, the corresponding conversion profiles are plotted for each one of the individual phenolic acids in various catalytic systems: (a) $Mn/TiO_2–CeO_2$, (b) $Cu/TiO_2–CeO_2$, (c) Mn–Ce–O, (d) Mn–Cu–O, and (e) $TiO_2–CeO_2$.

As can be seen from the individual profiles illustrated in Fig. 3, manganese and copper metals supported on titanium/cerium oxides were the ones with higher detoxification rates, see Fig. 3a and b. Once more, their catalytic activity did not depend on the catalyst preparation method. After 1 h of oxidation performed with $Mn/TiO_2–CeO_2$ catalyst, the conversions were 95.2, 94.1, 90.2, 86.0, 74.3, and 62.2% for syringic, vanillic, 3,4,5-trimethoxybenzoic, veratric, protocatechuic and *trans*-cinnamic acids, respectively, whereas with $Cu/TiO_2–CeO_2$ catalyst, were detected 95.1, 93.7, 89.8, 85.0, 73.7 and 61.6% of phenol-like pollutant degradation. These slight differences were of the same order of those observed in Fig. 1b, which reinforced the higher catalytic activity of $Mn/TiO_2–CeO_2$ and $Cu/TiO_2–CeO_2$ catalysts in comparison with single Mn–Cu–O and Mn–Ce–O catalysts. The least active catalytic promoter was $TiO_2–CeO_2$ demonstrating the lowest abatement efficiencies at 150 °C and 5 bar.

Apart from the above-mentioned decreasing orders of catalytic activity in terms of total organic carbon depletion, remarkable kinetic facts have been identified for the individual phenolic acid oxidation. A noteworthy behavior was detected in Fig. 3a–e which showed an interesting effect that is related with the overall conversion attained after 120 min. As can be observed, the five different catalytic formulations $Mn/TiO_2–CeO_2$, $Cu/TiO_2–CeO_2$, Mn–Ce–O, Mn–Cu–O, and $TiO_2–CeO_2$ have revealed distinctive detoxification rates. Having analyzed the normalized total organic carbon concentration as a function of time for these laboratory-made catalysts in Fig. 1b, slightly different oxidation profiles can be noticed with higher conversions in terms of total organic carbon concentration. However, the individual catalytic peroxide oxidation of each phenolic acid revealed that the abatement is incomplete and typically below 79.6% for the same oxidation time. This fact has been reported in literature as a co-oxidation phenomenon and it has been also observed recently for manganese/cerium catalysts [22]. Most importantly, when accomplishing novel wet peroxide oxidation with manganese

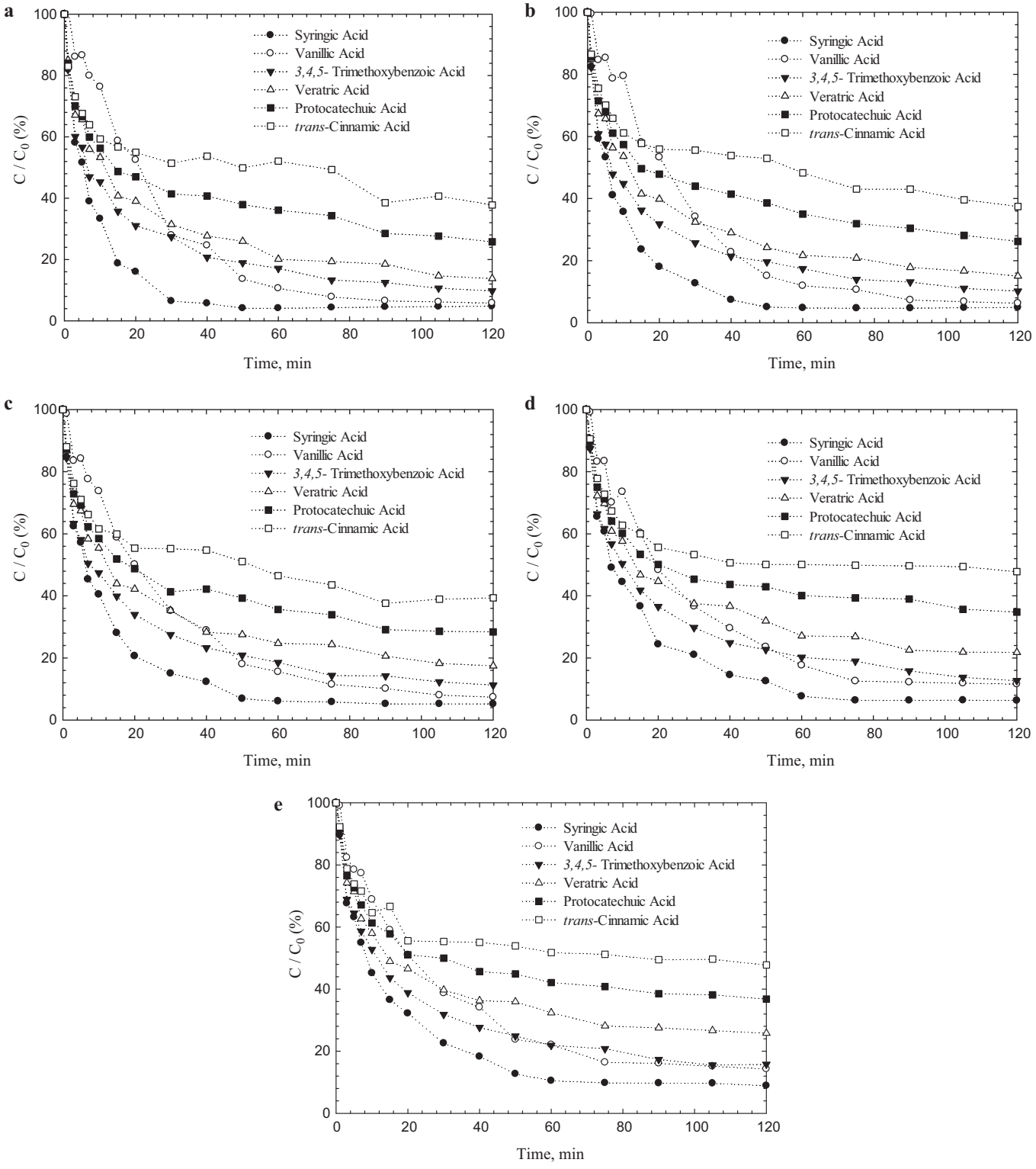

Fig. 3. Individual phenolic acids oxidation for different catalytic systems (6 g/L, 150 °C, 5 bar): (a) $Mn/TiO_2–CeO_2$, (b) $Cu/TiO_2–CeO_2$, (c) Mn–Ce–O, (d) Mn–Cu–O, and (e) $TiO_2–CeO_2$.

and copper metals supported on titanium/cerium oxides, these catalytic runs unveiled a notable co-oxidation phenomenon of the phenolic mixture. This fact can be explained by inferring the oxidation pathway of a phenolic compound that followed the formation of free-radical intermediates produced from another phenolic compound. Indeed, the relationship between the depletion profiles of the organic compounds during wet peroxide oxidation of liquid pollutant mixtures has a strong influence on the detoxification efficiencies as reported by Figs. 1 and 3.

The aforementioned kinetic phenomenon can in all likelihood be ascribed to the attainment of synergetic interactions between the individual phenol-like compounds. Provided that the catalytic activity is negatively affected by the single abatement of each phenolic acid, here an assortment of aromatic or even other organic

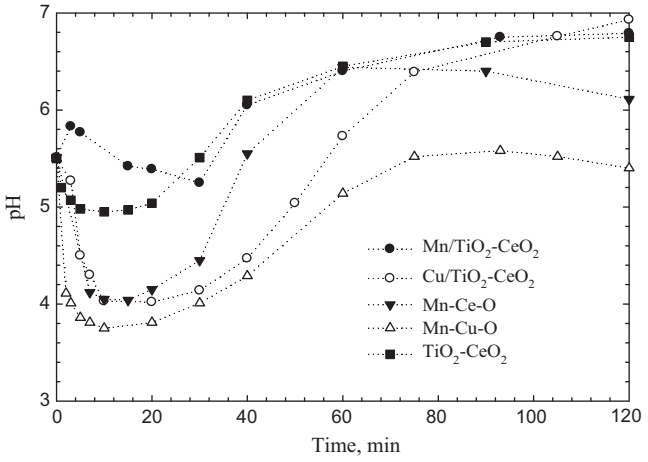

Fig. 4. pH profiles of the reaction solution at 150 °C, 5 bar and 6 g/L catalyst concentration for: $Mn/TiO_2–CeO_2$, $Cu/TiO_2–CeO_2$, Mn–Ce–O, Mn–Cu–O, and $TiO_2–CeO_2$.

acidic compounds may speed up the oxidation rate due to the synergism between pollutants as reported elsewhere [23] on the subcritical aqueous-phase oxidation kinetics of unsaturated carboxylic acids such as acrylic, maleic, fumaric, and muconic acids. It is worth remarking that these low molecular weight compounds has been identified as intermediate products in wet oxidation of phenols and a homogeneous radical mechanism is generally proposed as the reaction pathway. As long as our case-study encompassed an advancement to wet peroxide oxidation, higher decontamination rates have been attained under milder operating conditions. Moreover, there has been reported in the literature indirect experimental evidence of co-oxidation [24,25] claiming that the observed rate of oxidation for a mixture of high- and low-molecular-weight poly(ethylene glycol)s is much higher than the theoretical rate of oxidation and claimed that the oxidation reaction is free radical in nature and the active free-radical species produced from the more-fragile polymers attack low-molecular-weight and accelerate the reaction. Likewise, this phenomenon has been used as one method to indirectly determine if free-radical reactions are occurring during wet oxidation [12]. Specifically, syringic acid was the most reactive phenolic acid pollutant being promptly oxidized during the first 30 min of reaction time with $Mn/TiO_2–CeO_2$ and $Cu/TiO_2–CeO_2$ catalysts; proceeding further after 60 min for Mn–Ce–O, Mn–Cu–O and $TiO_2–CeO_2$ oxides. Special consideration was paid to the initial reaction times so the higher oxidation rates were obtained as expected from a synergetic-interaction regime, and afterwards the conversion profile shifted gradually concerning to the formation and degradation of intermediate compounds with lower refractory characteristics. Alternatively, *trans*-cinnamic acid exhibited the lower depletion rates for both laboratory-made catalysts. After 2 h, the conversions were 62.2, 62.6, 60.7, 51.2, and 52.3% for $Mn/TiO_2–CeO_2$, $Cu/TiO_2–CeO_2$, Mn–Ce–O, Mn–Cu–O, and $TiO_2–CeO_2$, respectively.

3.3. pH and reaction intermediates

Aiming to gaining further insights into the reaction pathway, the pH of phenolic solutions was monitored during the wet peroxide oxidation runs for all laboratory-made catalysts. Fig. 4 depicts the transient evolution of reaction mixture pH at 150 °C and 5 bar for $Mn/TiO_2–CeO_2$, $Cu/TiO_2–CeO_2$, Mn–Ce–O, Mn–Cu–O, and $TiO_2–CeO_2$ catalysts with a concentration of 6 g/L. The entire range of catalytic wet peroxide oxidation experiments revealed an indistinguishable behavior with an initial pH decrease followed by a slight increase, namely for the manganese and copper metals supported on titanium/cerium oxides. The minimum value of pH (3.7) was also observed for the Mn–Cu–O catalyst whereas the maximum value (6.9) was detected for the $Mn/TiO_2–CeO_2$. In fact, the copper catalysts were the ones that exhibited a significant initial decrease of pH which can be related with the slower total organic carbon degradation rate observed in Fig. 1b for the same reaction time. Conversely, the $Mn/TiO_2–CeO_2$ and $TiO_2–CeO_2$ catalysts revealed a minor pH decrease during the initial reaction time period so the respective improvement in total organic carbon depletion was followed by a regular increase in pH. This fact can be underlined by the formation of end products as carbon dioxide and water, and after 1 h, when the organic content removal being almost complete reached a plateau, the corresponding pH increased slowly. Taking into account that phenol-like pollutants conferred initially an acid character to the reaction mixture, after 30 min it can be seen that $Mn/TiO_2–CeO_2$ catalyst was the one that exposed the highest value of pH close to the neutralization condition. This event was likely attributed to the enhanced abatement efficiencies which were related with the fastest pollutant degradation rate observed for that catalyst, see Fig. 1b. Therefore, these phenomena triggered higher values of pH toward the complete abatement of phenol-like compounds, in terms of carbon content, and neutralization, in terms of pH. In addition, slight pH profiles were detected for both Mn–Ce–O and Mn–Cu–O catalysts corresponding to the minor differences in the ultimate removal efficiencies.

Systematic research on reaction pathway can be also accomplished by evaluating the pH profiles and the reaction intermediates. The intermediate compounds concentration was monitored by HPLC during the wet peroxide oxidations. The acetic acid and phenol concentrations as a function of time for $Mn/TiO_2–CeO_2$, $Cu/TiO_2–CeO_2$, Mn–Ce–O, Mn–Cu–O, and $TiO_2–CeO_2$ catalysts are shown in Fig. 5 at 150 °C, 5 bar and 6 g/L. The ring cleavage and low weight carboxylic acid products were found as major intermediaries in the catalytic wet peroxide treatment; thereby the mechanism followed the decarboxylation reaction route of aromatic end groups leading to phenol formation, and an oxygen attack to the aromatic double bond resulting in the formation of intermediate compounds such as acetic acid. Indeed, as the reaction started the phenolic acids are oxidized to low molecular weight carboxylic acids and other open-ring intermediate compounds. The most representative carboxylic acid that was followed by means of HPLC was acetic acid; however this acid was not present at the beginning of the oxidation runs. This means that the production of acetic acid as an intermediate compound arose from the aromatic ring cleavage of the initial pollutants. After the first 10 min, the intermediate compounds such as acetic acid and phenol were further oxidized to carbon dioxide and water.

The experimental runs performed with $Mn/TiO_2–CeO_2$ and $TiO_2–CeO_2$ revealed a slight initial pH decrease as shown in Fig. 4 which can be related with the formation of low weight carboxylic acids such as acetic acid that were the reaction intermediates detected during the reaction course as depicted by Fig. 5. In fact, in the first 15 min of reaction the concentration profiles for acetic acid and phenol shown in Fig. 5 indicated the major production rates of these intermediate compounds. Following the initial pH decrease, a further increase more pronounced for manganese/copper catalysts should be due to the formation of carbon dioxide and water. As the oxidation time progresses till 1 h, pH did not change considerably most likely due to the slower abatement efficiencies in both titanium and cerium catalysts. Most prominently, the $Cu/TiO_2–CeO_2$ and even the Mn–Ce–O catalysts gave us negligible variations for acetic acid and phenol concentration profiles being incrementally oxidized in the first hour of reaction time. Consequently, $Mn/TiO_2–CeO_2$ catalyst revealed the highest catalytic activity toward the complete abatement of phenol-like pollutants.

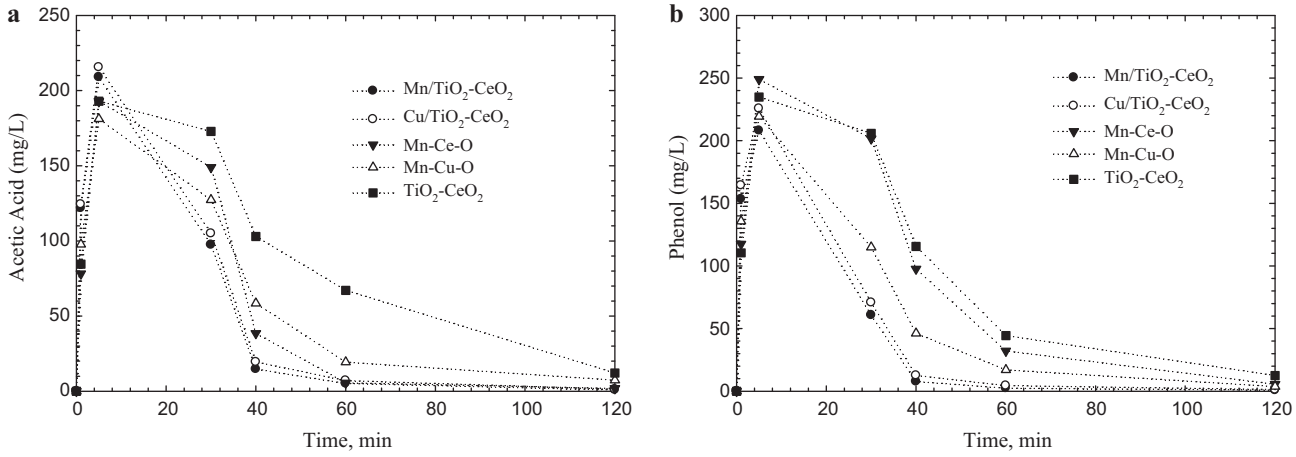

Fig. 5. (a) Acetic acid and (b) phenol concentrations as a function of time for: $Mn/TiO_2–CeO_2$, $Cu/TiO_2–CeO_2$, Mn–Ce–O, Mn–Cu–O, and $TiO_2–CeO_2$.

3.4. Catalysts stability in terms of leaching and carbon adsorption

Bearing in mind that the advancement of novel catalyst for wet peroxide oxidation should embrace a subsequent industrial implementation, the laboratory-made catalysts have not only to be active but it should be also stable in terms of premature deactivation. The most significant deactivation factors investigated in the literature are the active metal leaching from the catalytic structure to the liquid phase and the deposition of carbonaceous materials resulting in the irreversible loss of active sites through the poisoning of catalyst pores. It is well known that metal leaching to the bulk liquid can be relieved with the subsequent metal recovery step in order to purge this new pollution source, but its application requires a dedicated industrial unit encompassing relevant economical drawbacks.

In this realm, the manganese leaching was quantified by atomic absorption and the adsorption of carbonyl species on the catalyst surface was measured by elemental analysis after the oxidation runs. Table 2 reports the manganese concentration of the final aqueous solution after 120 min of oxidation catalyzed by $Mn/TiO_2–CeO_2$, $Cu/TiO_2–CeO_2$, Mn–Ce–O, Mn–Cu–O, and $TiO_2–CeO_2$. Here, no measurable differences were found for both manganese and copper metals supported on titanium/cerium oxides so that the preparation method had only a minor influence on the catalytic stability as discussed formerly. In spite of their higher activity, $Mn/TiO_2–CeO_2$ catalysts were the ones that exhibited the higher manganese solution concentrations in the treated effluent (1.84 mg Mn/L). Regarding the Mn–Ce–O and Mn–Cu–O, the highest value of manganese leaching was obtained with the cerium based catalyst, whereas the lowest value was attained with the copper based formulation. In addition, lower leaching levels were attained with the copper based catalysts; Mn–Cu–O exhibited 0.24 mg Cu/L whereas the $Cu/TiO_2–CeO_2$ leached 0.16 mg Cu/L. Hence, it seems that the higher catalytic activity verified for manganese and copper metals supported on titanium/cerium oxides in comparison with the copper oxides is also related with the integrated metal framework realized particularly by $Mn/TiO_2–CeO_2$.

Table 2
Mn and Cu leaching results to the liquid phase after 120 min for each metal based catalyst (150 °C and 5 bar, 6 g/L).

Catalyst	mg Mn/L	mg Cu/L
$Mn/TiO_2–CeO_2$	1.84	–
Mn–Ce–O	1.43	–
Mn–Cu–O	1.21	0.24
$Cu/TiO_2–CeO_2$	–	0.16

Another source of preliminary catalyst deactivation is linked with the carbon deposition on the catalyst surface. This event restricts the access of the reactants to active sites so elemental analysis was carried out after the recovery of the catalyst at the end of the experiments. The percentages of carbon weight found in the catalysts (%C, w/w), hydrogen (%H, w/w) and nitrogen (%N, w/w) are shown in Table 3 as well as the TOC adsorbed relatively to the initial TOC fed to the reactor and the TOC effectively oxidized after 120 min for each laboratory-made catalyst. According to these results, one may conclude that adsorbed carbon obtained is relatively low for both laboratorial and commercial catalysts. For instance, the weight percentage of 1.467% was obtained with the most active catalyst $Mn/TiO_2–CeO_2$ catalyst which corresponds to 3.37% of adsorbed carbon being possible to conclude that the overall abatement efficiency was 76.2%, see Fig. 1b. Practically, the initial TOC was converted to carbon dioxide and water and only a small fraction was adsorbed onto the catalyst. In what regards the other analyzed elements (H and N), only hydrogen was detected both in the manganese and copper catalysts supported on titanium and cerium oxides with no substantial effect on the catalytic stability.

3.5. XRD and BET analysis of catalysts

X-ray diffraction analysis was used to characterize the phase structure and the phase composition of the most active $TiO_2–CeO_2$ based catalyst. Fig. 6a and b shows the powder XRD patterns of the fresh and used $Mn/TiO_2–CeO_2$ catalyst. Having considered the main features of the titanium oxide patterns, the diffractogram revealed a titanium enriched catalyst. In fact, taking into account pure TiO_2, the peaks of anatase titania at $2\theta = 24.9°, 36.8°, 46.7°$, and $52.1°$ were detected. This characterization profile means that $Mn/TiO_2–CeO_2$ catalyst was synthesized as of a typical anatase structure. In titanium based catalysts, the peaks of anatase titania became much weaker and the wider with the increase of adding cerium content into titanium oxide support, while no peaks of copper oxides were observed in the spectra of X-ray diffraction. Notwithstanding the crystal size of $Mn/TiO_2–CeO_2$ was lower with the addition of cerium oxide the surface area remained roughly identical. The incorporation of CeO_2 was found to produce an amorphous phase so the diffractogram exhibited the most asymmetric peaks. A possible reasoning for this event is that it can be associated with large lattice distortion resulting from the introduction of dopant/vacancy sites. Moreover, the resilient peaks for pure cerium oxide were ascribed to cubic CeO_2 at $2\theta = 27.4°$, $32.5°$, $46.7°$, and $55.4°$ as supported by preliminary characterizations which have indicated the intrinsic diffraction peaks of cerianite CeO_2. Here, the X-ray diffraction

Table 3
Carbon concentration adsorbed in the catalyst, initial TOC percentage adsorbed and effectively oxidized after 120 min for each laboratory-made catalyst (150 °C, 5 bar, 6 g/L).

Catalyst	%C (w/w)	%H (w/w)	%N (w/w)	$\%TOC_{adsorbed}$	$\%TOC_{oxidized}$
$Mn/TiO_2–CeO_2$	1.467	2.975	<0.01	3.37	76.2
$Cu/TiO_2–CeO_2$	1.121	3.261	<0.01	3.21	71.1
Mn–Ce–O	1.875	1.294	<0.01	4.08	66.5
Mn–Cu–O	0.976	0.987	<0.01	3.07	54.4
$TiO_2–CeO_2$	2.108	2.908	<0.01	4.62	43.3

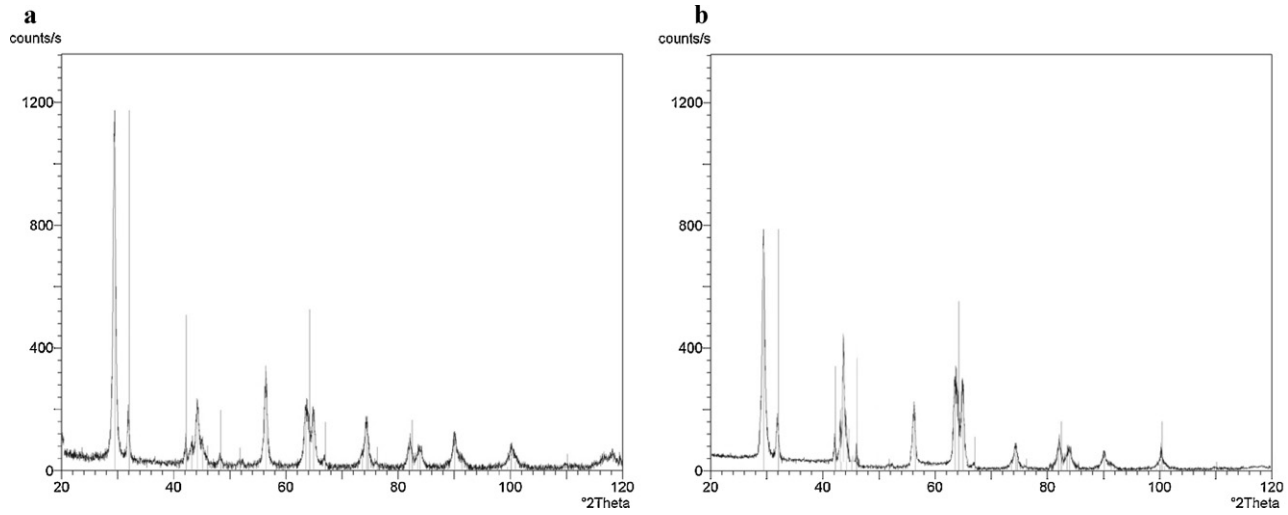

Fig. 6. X-ray diffractogram of (a) fresh and (b) used $Mn/TiO_2–CeO_2$ catalyst.

analysis pointed out the absence of titanium oxide that arose experimentally from the generation of metal solutions characterized by cerianite structure and most importantly due to an amorphous titanium oxide phase.

The BET isotherm for the $Mn/TiO_2–CeO_2$ catalyst before and after 2 h of catalytic wet peroxide oxidation was determined through the accelerated surface area and porosimetry analyzer. Both isotherms show a hysteresis loop for high range of relative pressure which is related with the capillary condensation and/or evaporation in mesoporous structures as depicted in Fig. 7a. After performing catalytic wet peroxide oxidations with the $Mn/TiO_2–CeO_2$, the Brunauer–Emmet–Teller surface area (S_{BET}) decreased slightly from 197.1 to 192.9 m^2/g, corresponding to a decrease of 2.1%. From the pore size distribution analysis plotted in Fig. 7b, an average pore diameter decreased from 0.0321 to 0.0369 μm (pore sizes corresponding to mesoporous/macroporous) was observed from the fresh to the spent catalyst. According to the preceding fact on a mesoporous/macroporous structure, both fresh and used materials exhibited pores with diameters in the range of 0.0038 and 0.1 μm. Additionally, one should mention that the mercury porosimetry was better designed to characterize pores with diameters higher than 7 nm, which requires a maximum intrusion pressure of 30,000 psia, thereby the average pore diameters are most likely lower than the reported characterization parameters.

3.6. TEM and SEM catalyst characterization

Two representative TEM photographs are depicted in Fig. 8 of fresh and used $Mn/TiO_2–CeO_2$ catalyst. According to these patterns, asymmetrical particles were found with the most active catalyst in where it can be observed pertinent aggregates and clusters of titanium and cerium oxide particles. A enhanced or quasi-homogeneous distribution was attained by enriched the catalyst backbone with cerium oxide. This is mainly attributed to the integration of the lanthanide into the lattice framework of titanium oxide. Additionally, the better homogeneous phases can be achieved with an optimized substitution of titanium which ultimately revealed the absence of cerium oxide diffraction peaks. Concomitantly, the manganese metal is included into the existent lattice of titanium oxide so the superior homogenous frameworks have been obtained with $Mn/TiO_2–CeO_2$ catalysts.

The structural morphology of $Mn/TiO_2–CeO_2$ catalyst was also observed by means of scanning electron microscopy in fresh and used samples. Fig. 9 compares both fresh and used catalysts and, as it can be observed, no significant differences were found in the catalyst after the catalytic wet peroxide oxidations for the most representative scale and magnification. Nevertheless, the manganese and cerium oxides (Mn–Ce–O), which have been previously investigated in catalytic wet oxidation, revealed dissimilar properties with respect to $Mn/TiO_2–CeO_2$. In that case, microscopic filaments with different lengths were formed on the catalyst surface. These whiskers were identified as MnOOH and/or MnO_2 during the catalytic abatement of carboxylic acids [26] and a mixture of phenolic acids typically found in olive oil mill wastewaters [22].

3.7. Sequential feed-batch performance

In order to evaluate how the TOC abatement is related with H_2O_2 conversion and CO_2 production, Table 4 shows the reaction results obtained at 150 °C, 5 bar with 6 g/L. As can be seen, the higher

Table 4
Reaction results at 150 °C, 5 bar, with 6 g/L catalyst.

Catalyst	TOC conversion (%)	H_2O_2 conversion (%)	CO_2 production (%)
$Mn/TiO_2–CeO_2$	79.6	58.9	90.4
$Cu/TiO_2–CeO_2$	74.3	54.0	84.8
Mn–Ce–O	70.5	50.4	80.7
Mn–Cu–O	57.5	38.4	66.5
$TiO_2–CeO_2$	47.9	29.6	55.8

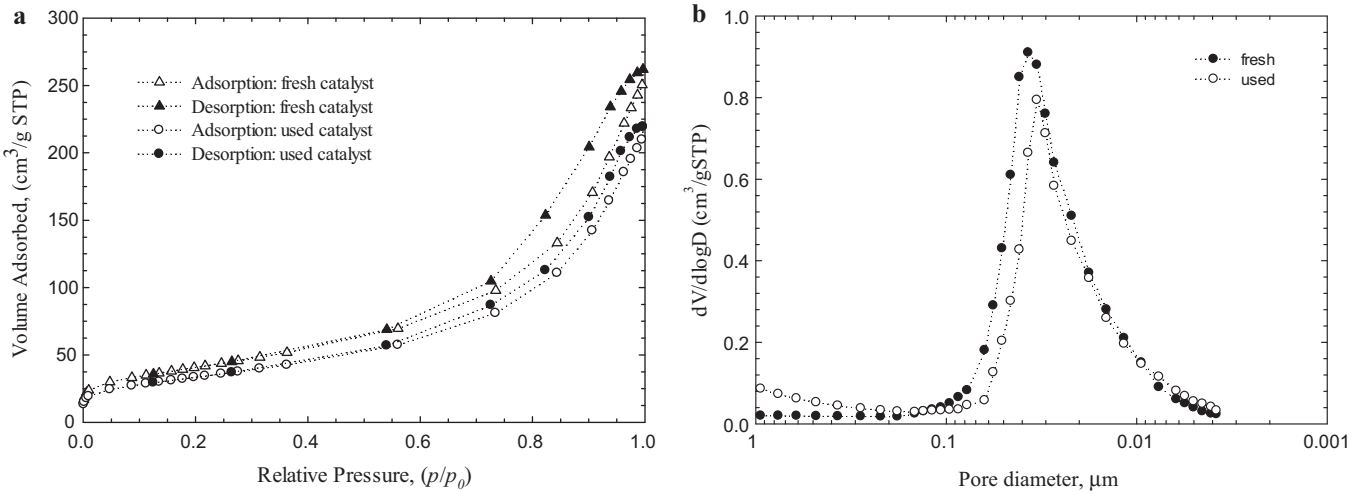

Fig. 7. Fresh and used $Mn/TiO_2–CeO_2$ catalyst: (a) BET isotherm and (b) pore size distribution with mercury porosimetry.

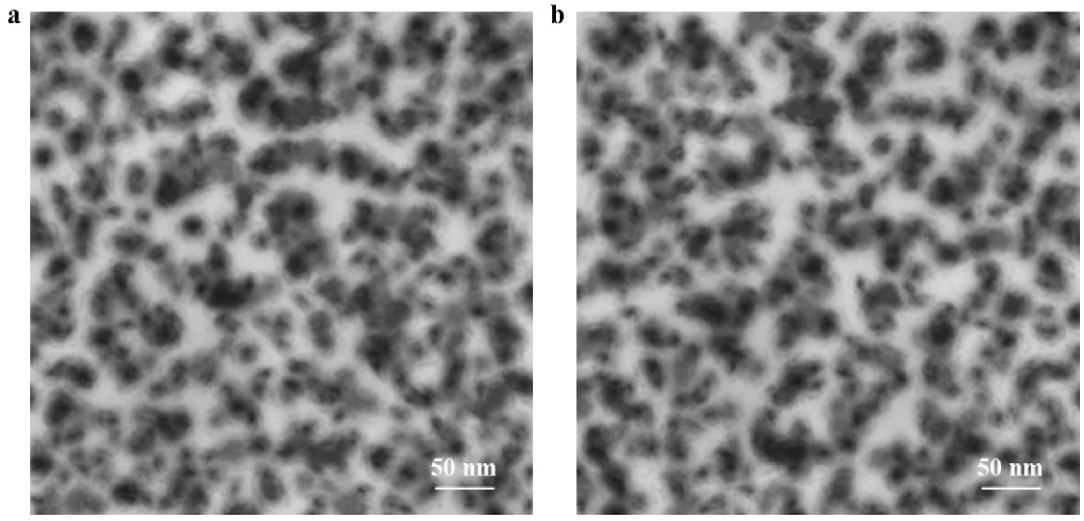

Fig. 8. Transmission electron microscopy patterns of (a) fresh and (b) used $Mn/TiO_2–CeO_2$ catalyst.

hydrogen peroxide conversions were attained with the following decreasing order: $Mn/TiO_2–CeO_2$, $Cu/TiO_2–CeO_2$, Mn–Ce–O, and $TiO_2–CeO_2$. This is also evidenced by the CO_2 productions that have been achieved at the same operating conditions. Apart from the physicochemical characterization techniques to evaluate the catalyst stability, particular attention was focused on how the $Mn/TiO_2–CeO_2$ catalyst preserves the abatement activity in terms of total organic carbon. A performance indicator encompasses the catalyst reuse during several hours of wet peroxide oxidation experiments. In this regard, the $Mn/TiO_2–CeO_2$ catalyst was recycled along sequential feed-batch trials to evaluate if its detoxification efficiencies remained at a similar level or if it

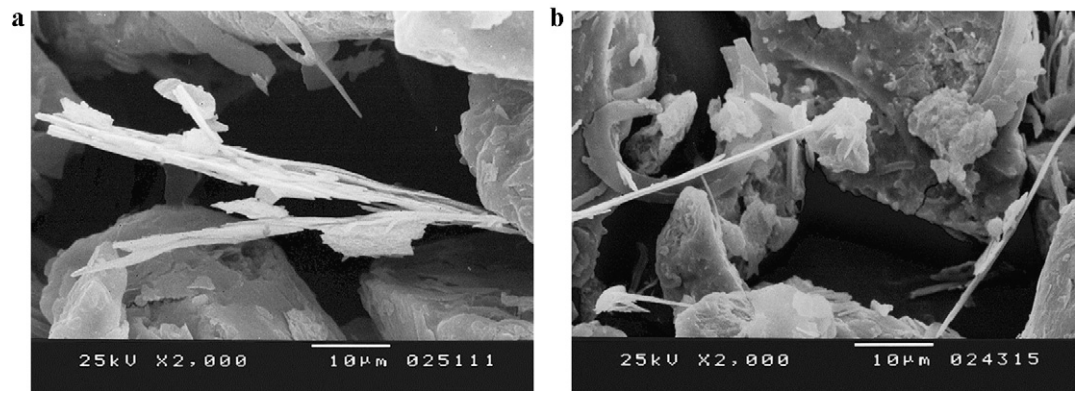

Fig. 9. Scanning electron microscopy patterns of (a) fresh and (b) used $Mn/TiO_2–CeO_2$ catalyst.

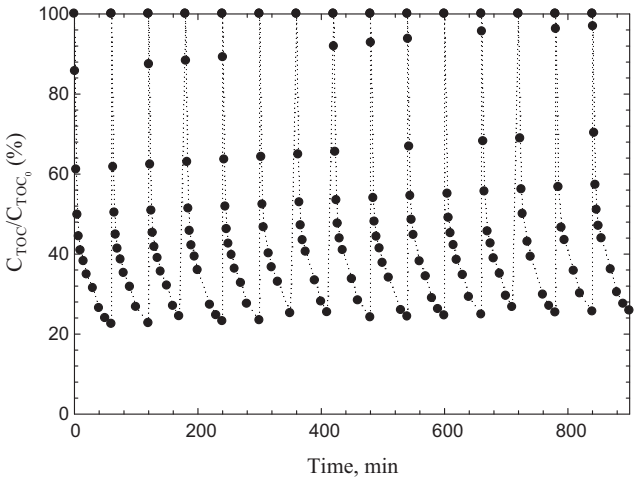

Fig. 10. Normalized total organic carbon concentration as function of time for a sequential batch experiment with phenolic mixture injection each 60 min.

is negatively affected on the catalytic activity performance. Systematic injections after 2 h of reaction time of a pre-calculated phenol-like pollutants solution were carried out in order to obtain a concentration close to the starting value. The total organic carbon concentration was measured during several experimental runs and the results are shown in Fig. 10. Even though the surface area from BET analysis decreased slightly from 197.1 to 192.9 m^2/g the detoxification rate in terms of total organic carbon concentration was approximately identical during the first six experimental runs. Furthermore, the Mn/TiO_2–CeO_2 catalytic system continuously demonstrated higher abatement efficiencies during the 10 min of each oxidation run. This fact is systematically reinforced by 67% of overall conversion for the majority of catalytic feed-batch trials.

4. Conclusions

At 150 °C, 5 bar only 13.9% in TOC abatement was achieved with wet oxidation and 26.4% for wet peroxide oxidation. Given that non-catalytic treatments were not able to mineralize efficiently the phenol-like pollutants, several laboratory-made catalysts: Mn/TiO_2–CeO_2, Cu/TiO_2–CeO_2, Mn–Ce–O, Mn–Cu–O, and TiO_2–CeO_2 were investigated in terms of catalytic activity and for individual phenolic compounds depletion. The manganese and copper metals supported on titanium and cerium oxides were found to be the most active toward the complete detoxification. These catalysts triggered the synergism events which highlighted the free-radical reaction pathway of wet peroxide oxidation by analysing the pH profiles and reaction intermediates. The catalytic stability was evaluated by metal leaching and carbon adsorption techniques and pointed out the Mn/TiO_2–CeO_2 catalyst as an appropriate and stable performer. The physicochemical characterization of Mn/TiO_2–CeO_2 and Cu/TiO_2–CeO_2 was accomplished through X-ray diffraction, BET, SEM and TEM analyses. Here, the integration of the lanthanide into the lattice framework of titanium oxide can explain the superior activity and enhanced homogenous catalytic framework attained with Mn/TiO_2–CeO_2. Additionally, this catalyst was applied during long term catalytic runs exhibiting practically the same abatement efficiencies. Consequently, the manganese metal supported on titanium and cerium oxides was identified as a remarkable formulation with further industrial implementation in catalytic wet peroxide oxidation of phenol-like pollutants.

Acknowledgment

The authors gratefully acknowledged the financial support of *Fundação para a Ciência e Tecnologia*, Portugal.

References

[1] P.L. Mills, R.V. Chaudhari, Catal. Today 48 (1999) 17–29.
[2] P. Paraskeva, E. Diamadopoulos, Olive mill waste management, Literature Review and Patent Survey, Typothito-George Dardanos Publications, Athens, Greece, 2004.
[3] M. DellaGreca, F. Previtera, A. Zarrelli, Phytochem. Anal. 15 (2004) 184–188.
[4] P. Paraskeva, E. Diamadopoulos, J. Chem. Technol. Biotechnol. 81 (2006) 1475–1485.
[5] N. Inchaurrondo, J. Cechini, J. Font, P. Haure, Appl. Catal. B: Environ. 111–112 (2012) 641–648.
[6] S.K. Bhargava, J. Tardio, J. Prasad, K. Foger, D.B. Akolekar, S.C. Grocott, Ind. Eng. Chem. Res. 45 (2006) 1221–1258.
[7] C. de Leitenberg, D. Goi, A. Primavera, A. Trovarelli, G. Dolcetti, Appl. Catal. B: Environ. 11 (1996) L29–L35.
[8] S. Imamura, H. Matsushige, N. Kawabata, T. Inui, Y. Takegami, J. Catal. 78 (1982) 217–224.
[9] A. Pintar, J. Levec, Catalytic oxidation of organics in aqueous solutions. 1. Kinetics of phenol oxidation, J. Catal. 135 (1992) 345–357.
[10] S. Hamoudi, A. Sayari, K. Belkacemi, L. Bonneviot, F. Larachi, Catal. Today 62 (2000) 379–388.
[11] L. Oliviero, J. Barbier, D. Duprez, A. Guerrero-Ruiz, B. Bachiller-Baeza, I. Rodriquez-Ramos, Appl. Catal. B: Environ. 25 (2000) 267–275.
[12] J. Tardio, S. Bhargava, S. Eyer, M. Sumich, D.B. Akolekar, Ind. Eng. Chem. Res. 43 (2004) 847–851.
[13] K. Belkacemi, F. Larachi, S. Hamoudi, G. Turcotte, A. Sayari, Ind. Eng. Chem. Res. 38 (1999) 2268–2274.
[14] L. Lei, X. Hu, P. Yue, Water Res. 32 (1998) 2753–2759.
[15] C. Catrinescu, C. Teodosiu, M. Macoveanu, J. Miehe-Brendlé, R. Le Dred, Water Res. 37 (2003) 1154–1160.
[16] P. Massa, A. Dafinov, F. Medina Cabello, R. Fenoglio, Catal. Commun. 9 (2008) 1533–1538.
[17] A. Quintanilla, N. Menéndez, J. Tornero, J.A. Casas, J.J. Rodríguez, Appl. Catal. B: Environ. 81 (2008) 105–114.
[18] M. Neamţu, C. Zaharia, C. Catrinescu, A. Yediler, M. Macoveanu, A. Kettrup, Appl. Catal. B: Environ. 48 (2004) 287–294.
[19] Y. Liu, D. Sun, J. Hazard. Mater. 143 (2007) 448–454.
[20] N. Mulinacci, C. Galardi, P. Pinelli, F.F. Vincieri, J. Agric. Food Chem. 49 (2001) 3509–3514.
[21] A. Silva, I. Castelo-Branco, R. Quinta-Ferreira, J. Levec, Chem. Eng. Sci. 58 (2003) 963–970.
[22] R.J.G. Lopes, A. Silva, R. Quinta-Ferreira, Appl. Catal. B 73 (2007) 193–202.
[23] R. Shende, J. Levec, Ind. Eng. Chem. Res. 39 (2000) 40–47.
[24] D. Mantzavinos, A.G. Livingston, R. Hellenbrand, I.S. Metcalfe, Chem. Eng. Sci. 51 (1996) 4219–4235.
[25] M.J. Birchmeier, C.G. Hill, C.J. Houtman, R.H. Atalla, I. Weinstock, Ind. Eng. Chem. Res. 39 (2000) 55–64.
[26] A. Silva, R. Marques, R. Quinta-Ferreira, Appl. Catal. B 47 (2004) 269–279.